Penetration of Lipid Membranes by Gold Nanoparticles: Insights into Cellular Uptake, Cytotoxicity, and Their Relationship

Jiaqi Lin,[†] Hongwu Zhang,[†,*] Zhen Chen,[†,‡] and Yonggang Zheng[†]

[†]State Key Laboratory of Structure Analysis for Industrial Equipment, Department of Engineering Mechanics, Faculty of Vehicle Engineering and Mechanics, Dalian University of Technology, Dalian 116024, P. R. China, and [‡]Department of Civil and Environmental Engineering, University of Missouri, Columbia, Missouri 65211-2200

ABSTRACT Nanoparticle penetration into cell membranes is an interesting phenomenon that may have crucial implications on the nanoparticles' biomedical applications. In this paper, a coarse-grained model for gold nanoparticles (AuNPs) is developed (verified against experimental data available) to simulate their interactions with model lipid membranes. Simulations reveal that AuNPs with different signs and densities of surface charges spontaneously adhere to the bilayer surface or penetrate into the bilayer interior. The potential of mean force calculations show that the energy gains upon adhesion or penetration is significant. In the case of penetration, it is found that defective areas are induced across the entire surface of the upper leaflet of the bilayer and a hydrophilic pore that transports water molecules was formed with its surrounding lipids highly disordered. Penetration and its concomitant membrane disruptions can be a possible mechanism of the two observed phenomena in experiments: AuNPs bypass endocytosis during their internalization into cells and cytotoxicity of AuNPs. It is also found that both the level of penetration and membrane disruption increase as the charge density of the AuNP increases, but in different manners. The findings suggest a way of controlling the AuNP—cell interactions by manipulating surface charge densities of AuNPs to achieve designated goals in their biomedical applications, such as striking a balance between their cellular uptake and cytotoxicity in order to achieve optimal delivery efficiency as delivery agents.

KEYWORDS: AuNPs (gold nanoparticles) · lipid bilayer · penetration · membrane disruption · cellular uptake · cytotoxicity

The biomedical applications of gold nanoparticles (AuNPs) to be used as delivery, diagnostic, and therapeutic agents have been growing rapidly over recent years.[1−5] Their efficiency of transporting DNA to nucleus is 8 times higher than that of polyethylenimine.[6] They have also been successfully utilized in novel cancer therapies.[7] In most of these bioapplications, the nanoparticles are required to pass cell plasma membranes either by endocytosis[8] or by direct penetration to reach target cellular compartments, during which significant toxic effects may be induced to the cells.[9] Safe and efficient localization of nanoparticles is critical for these bioapplications, which partly leads to the rising of a new field, nanotoxicology.[10,11] Controlling the balance between efficiently crossing cell membranes and the nanoparticles potential toxic effect is one of the key challenges in designing and fabricating these synthetic nanoparticles.[12]

Numerous experimental studies have been conducted to probe AuNP-cell interactions in the past few years. It has been reported that the sign of surface charges can dramatically influence the uptake of AuNPs.[13] In addition, different shapes,[14] ligand structures,[15] and compositions[16] of AuNPs can also lead to different levels of cellular uptake. In particular, it is found that cationic and anionic AuNPs follow different internalization pathways (endocytosis or penetration of cell membrane) to enter cells.[13] Interestingly, surface-structure-regulated anionic AuNPs can bypass endocytosis without overtly disrupting cell membranes.[17] However, the mechanism of AuNP uptake is still poorly understood. On the other hand, while cytotoxicity measurements give astounding results of AuNPs with different physical and chemical characters,[18−20] the principles underlying AuNPs' cytotoxicity is not yet established. The lack of atomic-level details on AuNP−cell membrane interactions prevent us from gaining an in-depth understanding of the observed phenomena. In addition, the differences in experimental procedures and characterizations of AuNPs make the current results difficult to be normalized, which yield a necessity for a systematic study on the AuNP−cell membrane interactions.[21]

In this paper, we probed the interactions between AuNPs and cell membranes by means of molecular dynamics (MD)

*Address correspondence to zhanghw@dlut.edu.cn.

Received for review May 17, 2010 and accepted August 18, 2010.

Published online August 27, 2010. 10.1021/nn1010792

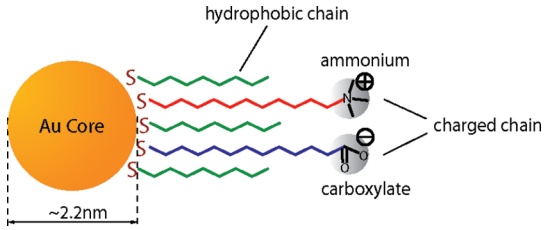

Figure 1. A schematic illustration of the structure of the AuNP. The alkyl thiol ligand terminals of the AuNP are functionalized with ammonium or caroxylate groups to feature positive or negative surface charges.

simulation. Previous simulation studies of AuNPs have illustrated their ligand dynamics,[22] solvent effect, and the interaction between two AuNPs.[23] To the authors' knowledge, however, their interactions with lipid membranes have not yet been investigated with MD simulation. Nevertheless there are papers concerning the interactions of cell membranes with other classes of widely used nanoparticles (*e.g.*, carbon nanotubes,[24] dendrimers,[25] and fullerenes[26]), which provide practical approaches and methodologies for the current study. Besides a typical zwitterionic lipid bilayer, we here first included the negative lipid bilayer in combination with a neutral bilayer to model typical mammalian cell membranes that possess an overall negative electric feature.[27] Derived from a widely used force field,[28] our coarse-grained (CG) model of AuNPs is atomistically informed and experimentally validated. The study reported here has examined the AuNP−membrane interactions under various conditions. The findings provide a mechanistic explanation for the observed cellular uptake and cytotoxicity of the AuNPs in experiments, and also suggest a procedure of controlling AuNP−cell interactions by manipulating surface charge densities of AuNPs to achieve certain goals in their biomedical applications.

RESULTS AND DISCUSSION

Figure 1 illustrates the structure of AuNPs in simulations. The ligand terminals of the nanoparticle are functionalized with different groups to feature different signs of surface charges. In potential of mean force (PMF) calculations and their corresponding unbiased simulations, charged AuNPs have 70% cationic or anionic coverage, which means they have 76 functionalized ligands (with ammonium or caroxylate terminals) and 32 unfunctionalized ligands (alkanes). Both an electronegative bilayer and an electroneutral bilayer are employed in our simulations. The neutral bilayer is composed of pure dipalmitoylphosphatidylcholine (DPPC), whereas the negative bilayer (PC/PG) is a mixture of DPPC and dipamitoylphosphatidylglycerol (DPPG) in a ratio of 3:1.

Free Energy Analysis. We began by obtaining the free energy profile of AuNP−membrane interactions in order to illustrate the thermodynamics of the system and the preferences of the AuNPs as they relate to the bilayers. PMF of AuNPs as a function of their *z*-distance from the bilayer center was calculated for six different cases (three kinds of AuNPs, cationic, hydrophobic, and anionic interact with two kinds of bilayers, DPPC and PC/PG; see Figure 2 for case assignment). The bilayers' preferences for the AuNPs are clearly interpreted by the PMF curves as shown in Figure 2. In cases 1, 2, and 6, trajectory snapshots show that the AuNPs bound to the bilayers at the end of the 40 ns unbiased simulations. Correspondingly, PMF curves in these cases have their minimum located around the bilayer. Note that these PMF curves tend to have a narrow well shape, indicating the probability of finding the AuNPs in the observed positions (snapshots) is very high. In case 2 and case 6, the AuNPs adhered to the bilayers surface, a situation which is comparable to the absorption of an acetylated fifth-generation polyamidoamine dendrimer onto a DPPC bilayer.[25] In case 3 and case 4 (hydrophobic AuNPs), the PMF curves are relatively flat but drop steeply at the bilayer interior. Although a lower PMF value suggests a higher probability for a AuNPs to be located at the corresponding position, the penetration of the AuNPs into the bilayer interior was not observed in the simulations. This can be attributed to the small energy barriers located between the AuNPs and the bilayers, which prevent the AuNPs from moving downward to reach the bilayer interior. The PMF profiles of the neutral AuNPs show agreement to that of fullerenes[26] for their hydrophobic nature, although the size of an AuNP is larger than that of a C_{60}. Interestingly, the AuNP shows a strong preference for the bilayer surface in case 5, indicating that an anionic AuNP may bind to a negative bilayer, which seems to be counterintuitive. The PMF results suggest that the total energy gain upon binding is significant, although in some cases the binding is not spontaneous and thus requires external forces. The results also show that the signs of AuNPs surface charges significantly affect their interactions with lipid membranes and that the electric features of the bilayers are also important. An experiment conducted by Goodman *et al.* indicated that cationic AuNPs are more disruptive to negative charged lipid vesicles than their anionic counterparts, whereas they both show similar levels of disruption to zwitterionic lipid vesicles, which shows qualitative agreement to our PMF calculations that the energy gain upon binding between cationic AuNPs and negative bilayers is the greatest.

Because different signs of surface charges of AuNPs lead to different outcomes, electrostatic interactions between AuNPs functional terminals and lipid head groups are expected to control the AuNP−bilayer interactions. This is confirmed by monitoring system potential energy fluctuations during the simulations. In cases 1, 2, and 6, where the binding between AuNPs and bilayers occurred, system Coulombic energy fluctuations are several times larger than Lennard-Jones (LJ) energy

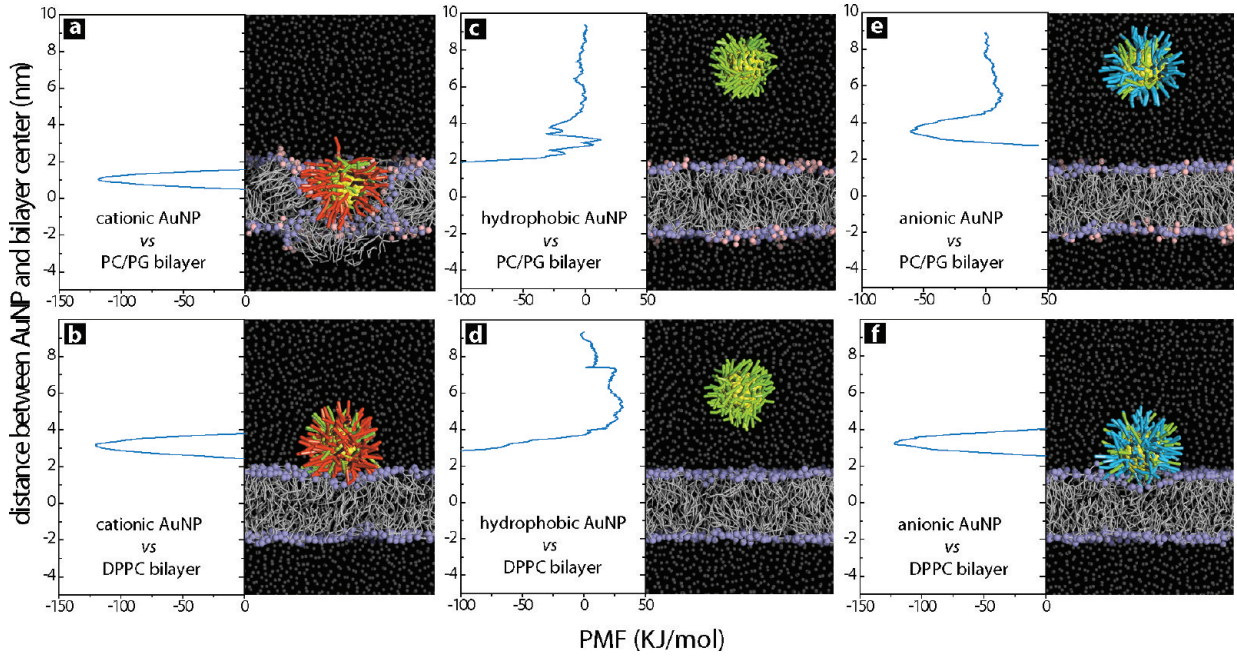

Figure 2. PMF profiles of cationic (a, b), hydrophobic (c, d) and anionic (e, f) AuNPs as a function of their distance from the center of DPPC (a, c, and e) and PC/PG (b, d, and f) bilayers. The left half of each graph is the PMF profile while the right is a trajectory snapshot of the equilibrated AuNP−bilayer system. Au core is shown in yellow, hydrophobic ligands in green, cationic ligands in red, anionic ligands in blue, DPPC head groups in ice blue, DPPG head groups in pink, lipids tails in sliver and water in transparent white. The AuNPs were initially placed 7 nm above the bilayer center. Each PMF curve is estimated by a 0.1 nm sampling interval. Panels a to f are sequentially assigned as case 1 to case 6.

fluctuations, indicating that electrostatic interactions are dominant over hydrophobic interactions (see Supporting Information, Table S2). In each case, long-range Coulombic potential accounts for most electrostatic interactions.

Penetration of Lipid Membranes by AuNPs. Figure 3 characterizes the structural properties of the disrupted bilayer, in which case penetration occurred (cationic AuNP *vs* PC/PG bilayer). As the AuNP moved to the interior of the bilayer, it generated a severely disruptive pore which in turn induced defective areas (areas on the bilayer surface which are absent of lipid head groups) and altered bilayer surface texture. Figure 3b is the top view of the disrupted PC/PG bilayer. The removal of the AuNP had resulted in a visible pore. The "pore" region of the bilayer is substantially hydrated and is water permeable (Figure 3d). The inward water flux across the pore is about 17 molecule/ns, which is comparable to the flux of a ~2 nm^2 hydrophilic pore generated on a lipid membrane by mechanical stretch.[29] Permeation of ions across the bilayer, however, was not observed throughout the simulation. The defective areas, totaling 10 nm^2, are generated across the entire surface of the upper leaflet of the bilayer,

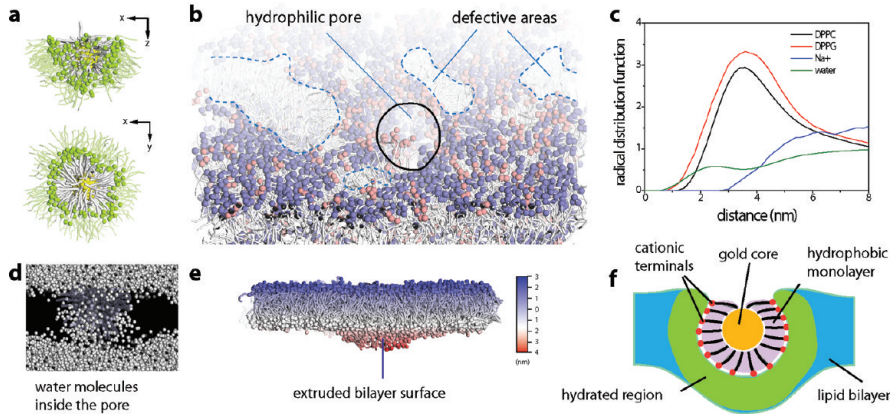

Figure 3. Structural changes of the cationic AuNP and the PC/PG bilayer upon binding. (a) Binding between the AuNP's ligand terminals and the lipid head groups. The lipids formed a shell to enwrap the AuNP. (b) A typical pore and defective areas were generated on the bilayer by the AuNP penetration. (c) Radial distribution functions of gold atoms with respect to DPPC, DPPG, water, and counterions for 20 ns. (d) The penetration of the AuNP makes the bilayer water permeable. (e) The lower leaflet of the bilayer extrudes to accommodate the penetration of the particle. (f) A schematic illustration of the AuNP−bilayer interface.

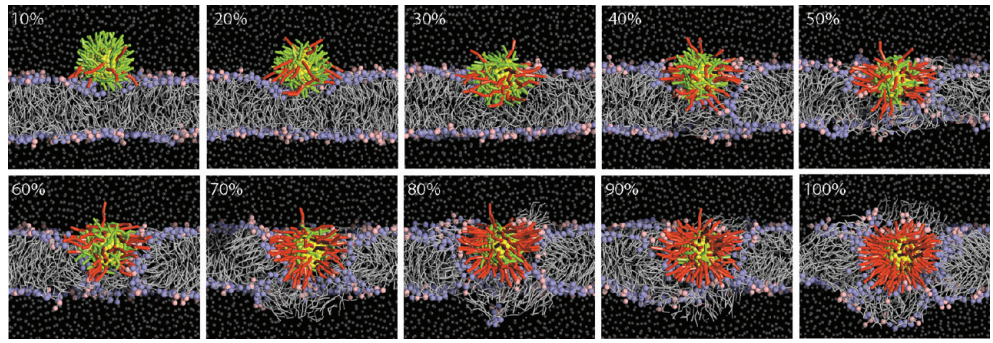

Figure 4. Interactions of AuNPs with different cationic surface charge densities with a PC/PG bilayer. Snapshots are taken at the end of every 40 ns MD simulation. Gold core is shown in yellow, hydrophobic ligands in green, cationic ligands in red, DPPC head groups in ice blue, DPPG head groups in pink, lipids tails in sliver, and water in transparent white. The percentage of cationic coverage of the AuNP is indicated in each snapshot.

causing direct contact between water molecules and the bilayer hydrophobic interior. In addition, the lower leaflet of the bilayer protruded downward to accommodate the penetration (Figure 3e). The implications of these disruptions are discussed in later sections. Figure 3c gives the radical distribution function of gold atoms with respect to lipids, ions, and water over 40 ns. Few water molecules can be found within 7 Å of the gold core, which means a hydrophobic environment was maintained inside the alkyl thiol monolayer (Figure 3f). Figure 3a shows that the ligands on the AuNP have reoriented themselves to adapt to the presence of the surrounding lipids. As a result, ligands on the upper surface of the AuNP are now horizontally aligned, which makes the top area uncovered with ligands. This may have certain implications to the cargo holding in drug delivery applications.[30] It is clear that the severe disruption on the bilayer is caused by the strong attractions between the terminals of AuNPs' cationic ligands (ammonium) and the phosphate groups of DPPC and DPPG. In a recent experiment, it is found that highly charged cationic AuNPs are able to generate holes on supported lipid bilayers.[33] These bilayers are supported on a mica surface, which carries negative net charges that provide the bilayer with a similar electric feature to that of a PC/PG bilayer. Although the size of holes observed in the experiment are larger than that the simulation, they both indicate a highly disruptive nature of cationic AuNPs shown to negative bilayers, which shows qualitative agreement to each other.

Effect of Surface Charge Density upon Penetration and Membrane Disruption. To investigate the effect of surface charge density of AuNP on the degree of penetration into the lipid membranes, we have constructed a group of AuNPs with different cationic coverage (percentage of ammonium-functionalized ligands on an AuNP), from 0% to 100% with an increment of 10%, to simulate their interaction with PC/PG bilayers. Simulation setup is identical to previously mentioned six cases. As illustrated in Figure 4, AuNPs bound to the PC/PG bilayer and induced deformation to it at all density values simulated. Both the level of penetration and disruption goes higher as the AuNPs' surface charge increases but in different manners. At the cationic coverage below 50%, the increase of the penetration is prominent. The particle is already "inside" the bilayer when the coverage has reached 50%. However, further increase of coverage promotes penetration to a much lesser degree. Even at 100% cationic coverage, the particle still resides in the bilayer interior and does not move downward to breakout the lower leaflet of the bilayer. By contrast, the disruption on the membrane is not significant until the coverage reaches around 60%. Further increase of coverage results in severe membrane disruption which is clearly visible. (The membrane disruption is quantified in the next paragraph.) At 100% cationic coverage, the bilayer formed a micelle to wrap the highly charged particle, and the surrounding regions of the membrane were substantially ruptured, which shows significant agreement to the continuum study.[31] For DPPC bilayers, although all the AuNPs with different cationic coverage did bind to the membrane, the effect of charge density is nonetheless insignificant on penetration (data not shown). The AuNP was not able to penetrate into the bilayer interior even at 100% cationic surface coating.

To give a quantitative picture of the relationship between AuNP penetration and membrane disruption, we have calculated several structural properties of the PC/PG bilayers, which are the root-mean-square deviation (rmsd), the average order parameter of lipid tails, the defective areas, and the inward water flux, as a function of AuNPs' cationic surface coating (Figure 5). As AuNPs' cationic coverage increases, the rmsd of the lipids rises monotonically from 0.9 to 1.5 nm, with minor fluctuations. The lipid average order parameter increases slightly at low cationic coverage (10% and 20%) and is moderately reduced at higher coverage. This slight increase can be attributed to the reconstruction of lipids toward a more ordered phase due to the absorption of a charged nanoparticle onto the membrane surface.[32] The defective areas on the bilayer are negli-

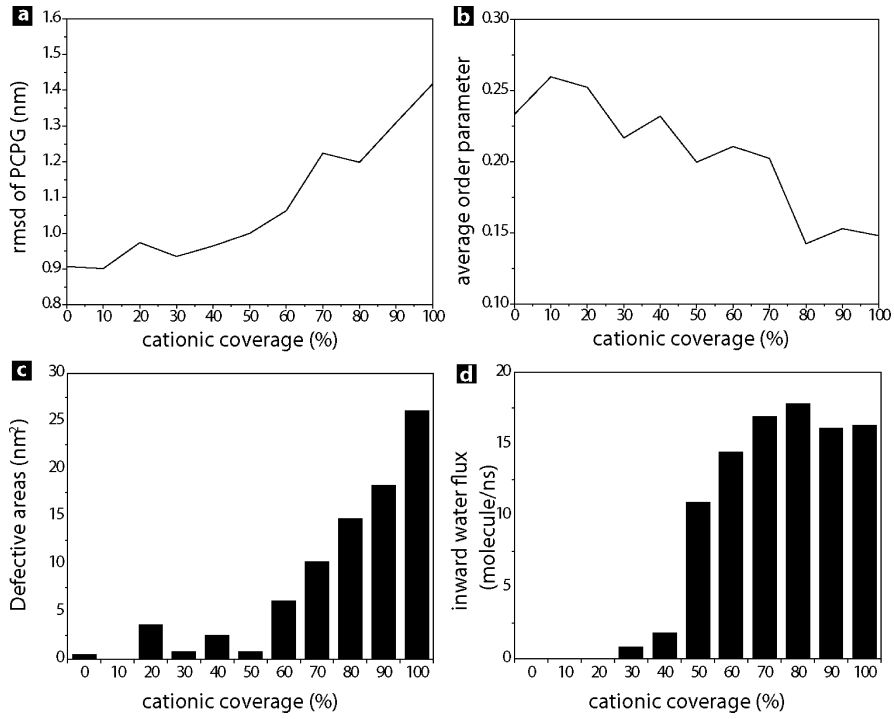

Figure 5. Changes of bilayer structural properties as a function of AuNP surface charge density: (a) The root-mean-square deviation of distance between lipids, (b) averaged order parameter of lipid tails, (c) defective areas (bilayer surface on which lipid head groups are absent), and (d) inward water flux (number of water molecules passed downwardly through the bilayer) during 40 ns simulation.

gible at the cationic coverage below 50% but begin to increase sharply from 50% at a rate of ~4 nm^2 per 10% coverage in a linear fashion. The result of inward water flux shows that the bilayer becomes permeable to water when the coverage reached 30% and the flux suddenly rises at 50% cationic coverage. However it subsequently increases slowly and remains at a level around 15 molecule/ns as the coverage maximizes, indicating the bilayer has a preference for discrete states in which water permeability remains relatively constant. Therefore, exceeding a certain threshold, in this case around 50% cationic coverage, of the surface charge density of AuNP would generate significant disruption to the lipid membranes.

Concluding from the above analysis, the influence of surface charge density of a AuNP on membrane can be divided into two stages. In the first stage where the AuNPs have lower charge densities, the effect of surface charge mainly contributes to penetration. In the second stage where AuNPs have higher charge densities, the effect of surface charge mainly contributes to membrane disruption since further penetration is not possible. The finding may provide us a clue on how to avoid high toxic effect of AuNPs while achieve certain goal in their biomedical applications.

Cellular Uptake of AuNPs. The sign of surface charge on AuNPs significantly affects the affinity constant between the particles and cell membranes. Typical mammalian cell membranes carry an overall negative charge,[27] which naturally leads to the assumption that the bulk of their regions are electronegative, while minority regions tend to have a neutral or positive electric feature. It can be learned from PMF analysis that the cationic AuNPs are strongly favored by the negative (PC/PG) bilayer, whereas the anionic AuNPs have to overcome an energy barrier in order to reach its surface, indicating that cationic AuNPs are much more likely to be absorbed onto the bilayer than their anionic counterparts. Since neutral bilayers have the same preference for the two kinds of AuNPs in PMF calculations, it is concluded that cationic AuNPs will have an overall higher membrane adhesion than their anionic counterparts on a typical mammalian cell membrane so long as the membrane tends to have an overall electronegative feature. A recent experimental study showed that the membrane affinity constant of cationic AuNPs is three times greater than that of anionic AuNPs in human cancer cell lines.[13] This result is promptly underpinned by the above analysis.

Furthermore, the aforementioned experiment discovered that the internalization rate of the cationic AuNPs is five times larger than that of the anionic AuNPs.[13] The authors demonstrated that two kinds of AuNPs are subjected to different internalization mechanisms: The anionic AuNPs are endocytosed into cells while half the amount of cationic AuNPs escape the endocytotic pathway. It is then postulated by the authors that these cationic AuNPs may directly diffuse into the cells by generating disruptions on the cell membranes, a hypothesis which has been proposed by several other

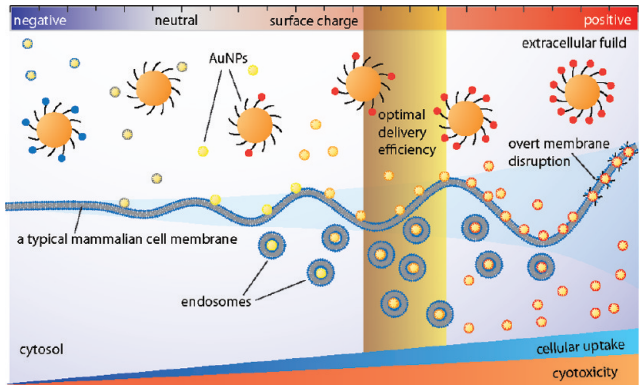

Figure 6. A schematic illustration indicating the effect of AuNPs' surface charge on their cellular uptake and cytotoxicity of a typical mammalian cell. Cationic AuNPs are favored by the cell membrane while anionic and hydrophobic AuNPs cannot reach the membrane easily. Increasing AuNP surface charge density will promote uptake but also raise cytotoxicity. Exceeding a threshold of surface charge density may have the AuNPs escape an endocytotic route and diffuse directly into the cytosol. Further increase of charge density may result in overt disruption of the membrane and thus cause acute toxic effect to cells. A certain amount of surface charge density may allow the AuNPs to strike a balance between cellular uptake and cytotoxicity to achieve optimal delivery efficiency.

recent publications.[17,33,34] Our simulations further corroborate this postulation by presenting insightful details. Cationic AuNPs with high surface charge densities can penetrate into the bilayer interior, generate a hydrophilic pore on it, and induce significant deformations to the surrounding lipids. Endocytosis, which is typically assisted by receptor-mediated formation of endosomes that enwrap the nanoparticles at the bilayer surface, is unlikely to occur when a AuNP is in such a deeply embedded position in the bilayer or when the surrounding region of the bilayer is severely disrupted.[35,36] Conversely, anionic AuNPs will merely be absorbed onto the bilayer surface (both negative and neutral bilayers, indicated by PMF profiles), creating an environment conducive to endocytosis.[35] The reason that half of cationic AuNPs in experiments did not escape endocytosis in the experiment is that they somehow have weaker interactions with the cell membranes (lower level of penetration, less membrane disruption) which are still within the grasp of the endocytotic mechanism. Further investigations are needed to understand the differences between the two internalization pathways.

Cytotoxicity of AuNPs. A recent experimental study reported that cationic AuNPs are, on average, 27 times more toxic than their anionic counterparts in three different cell lines.[16] Our simulations reveal two causes for this discrepancy: First, cationic AuNPs have higher adhesion to cell membranes than anionic AuNPs do, which is also a reason for their high uptake; second, their membrane disruption ability is far more significant than that of their anionic counterparts. AuNPs with high cationic surface coating can disrupt a bilayer membrane to a great extent, which subsequently compromises the membrane integrity and thus breach the hydrophobic barrier. The hydrated channel will lead to the exchange of medium between extracellular fluid and cytosol, which may cause acute cytotoxicity.[21] Although not enough to compromise bilayer integrity, anionic AuNPs are capable of altering cell functions by inducing changes on membrane protein properties as well as bilayer properties, which can in turn affect the functioning of membrane proteins (see ref 37 for an in-depth review). Changes on the functioning of membrane proteins are able to alter cell functions substantially, which may be one of the reasons for the observed minor cytotoxicity of anionic AuNPs, since the AuNPs are still able to induce negative effects once inside the cells.[9]

Relationship between Cellular Uptake and Cytotoxicity. Analysis of the experimental results indicates that cellular uptake and cytotoxicity of the AuNPs are in fact two linked factors which are jointly controlled by the surface charges of the AuNPs.[13,16] Simulation results give further information on how these factors are related to each other. For a typical mammalian cell membrane that carries a negative net charge, cationic AuNPs are more effective in interacting with cells than anionic AuNPs for their higher membrane adhesion (favored by either neutral or negative regions of the membrane), which is the reason that cationic AuNPs have much more clinical usages than their anionic counterparts.[21] Meanwhile, increasing AuNPs' cationic charge density will simultaneously promote both their cellular uptake and toxic effect, since higher densities will result not only in higher levels of adhesions (or even a quicker internalization pathway, *i.e.*, direct diffusion into cells) but also in increased disruptions to cell membranes, which may lead to acute cytotoxicity. The latter should be avoided in most AuNPs' biomedical applications. In the scenario of delivery applications, carefully tuning surface charge densities of the AuNPs can have them penetrate into the membrane while not generating significant membrane disruption, and thus can achieve a relative high uptake while not inducing acute cytotoxicity (Figure 6). A recent experiment has utilized cationic AuNPs to transfect DNA into mammalian cells.[6] It is found that an AuNP with cationic coverage of 68% is more effective in promoting transfection efficiency than AuNPs with other cationic coverage. Higher cationic coverage induces an overt toxic effect on cells that compromises the transfection efficiency of the AuNPs. This particular surface charge density of cationic AuNPs manages to strike a balance between uptake and cytotoxicity for the given cell type, thus resulting in a greater transfection efficiency than others. It should be noted that the payloads contained in or conjugated to AuNPs can also influence their interactions with cell membranes. Therefore there is great interest in studying the AuNP−membrane interactions with different cargos.

TABLE 1. Comparison of the Structural and Dynamical Properties of the CG AuNP Model with Experimental Data (Terrill *et al.*). C_8, C_{12}, and C_{16} are Octanethiol, Dodecanethiol, and Hexcanethiol Stabilized AuNPs, Respectively

	Au core radii (Å)[a]		radius of gyration (Å)[b]		diffusion coefficient[c]		average carbon distance (Å)[d] simulation		average carbon distance (Å)[d] experiment[32]	
	simulation	experiment[32]	simulation	experiment[32]	simulation	experiment[32]	$\langle X_{1-4} \rangle$	$\langle X_{5-8} \rangle$	$\langle X_{1-4} \rangle$	$\langle X_{5-8} \rangle$
C_8	11.136	10−13			1.333 ± 0.25	2.6 ± 0.3	3.643	6.849	3.250	6.597
C_{12}	11.136	10−13	11.45 ± 0.04	9.24 ± 0.05	0.918 ± 0.04	2.3 ± 0.2				
C_{16}	11.136	10−13			0.708 ± 0.12	1.6 ± 0.2				

[a]Radius of gold core was determined by averaging the distance between surface Au atoms and geometric center of the polyhedron with the addition of the radius of a single Au atom (1.44 Å). [b]Radius of gyration was calculated from C_{12} cluster in hexane. [c]Diffusion coefficients have a unit of 10^{-6} cm^2/s. They were calculated from the mean square displacements of AuNPs dissolved in chloroform over 64 ns. [d]Average carbon distance is the averaged normal distance of the *i*th carbon atom on octanethiols of C_8 from the gold−hydrocarbon interface (see Figure S1-d), which was calculated from the AuNP dissolved in hexane over 4 ns. See Supporting Information for details.

CONCLUSION

We have probed the interactions of AuNPs with model lipid membranes by CG MD simulations. A CG model of AuNPs is first constructed and verified against structural and dynamical properties of AuNPs measured in experiments. The simulation results reveal that different signs and densities of surface charge on AuNPs will result in either repulse of, adhesion to, or penetration into the lipid bilayers. PMF analysis shows that the adhesion and penetration are highly energy favorable while in the case of repulsion the particle is prevented from reaching the bilayer by small energy barriers. The binding between AuNPs and bilayers indicated to be mainly governed by the electrostatic interactions between the functionalized ligand terminals of the AuNPs and the bilayer head groups. It is found that upon penetration, a hydrophilic pore which transports water molecules is generated on the membrane, defective areas are induced across the entire surface of upper leaflet of the bilayer, and the lipids close to the nanoparticle are considerably disarranged. Both the cytotoxicity of the AuNPs and the bypass of the endocytotic pathway upon their internalization into cells observed in experiments are interpreted by the penetration of lipid membrane and its concomitant membrane disruption discovered in the simulation. It is also found that both the level of penetration and membrane disruption increase as the charge density of the AuNP increases, but in different fashions. The degree of penetration increases prominently at low charge densities while the membrane disruption begins to rise rapidly at higher charge densities. The finding suggests that it is possible to gain control over the interactions of AuNPs with cell membranes in order to promote their cellular uptake while minimizing their toxicity by carefully tuning their surface charges densities. The results provide critical information for AuNPs to achieve designated goals in their delivery, diagnostic, and therapeutic applications.

METHODS

The MARTINI force field[28] developed by Marrink *et al.* is employed in our simulations. The model is specialized in lipid membrane simulations and has recently been extended to include proteins.[38] The CG model is able to enhance computational efficiency by 3 orders of magnitude when compared to atomistic models.

Our CG AuNP model is compatible with the MARTINI force field. The gold core of the AuNPs is a truncated-octahedron[39] with a diameter of 2.2 nm and comprises 309 gold atoms. The three-dimensional monolayer that covers the gold core contains 104 alkyl thiol ligands. The CG AuNP model was constructed by three separate steps: obtaining the structure of the AuNP by atomistic MD simulations,[40] coarse-graining the atomistic model into CG beads, and calibrating the CG force fields to fit experimental data (see Supporting Information). Our CG AuNP model is faithful in reproducing several structural and dynamic properties of AuNPs in experiments.[41] These are the radius of gyration, the diffusion coefficient, and the average carbon distance (see Supporting Information, Figure S1-d for definition). We emphasize that our model is also capable of reflecting the difference between the ligands length (octanethiol, dodecanethiol, and hexadecanethiol) of AuNPs dissolved in organic compounds. Table 1 presents these properties of the AuNPs with simulation and experimental results. After coarse-graining, we added functional groups (ammonium and carboxylate) to ligand terminals of the AuNPs to introduce charges onto the nanoparticles for membrane simulations.

Two kinds of lipids, DPPC and DPPG, are involved in the present paper. DPPC is a typical lipid in the MATINI force field, which comprises 12 CG beads. DPPG has the same structure as DPPC but has a glycerol group instead of a choline group, which impels a negative net charge on the lipid. The neutral bilayer was created by self-assembling DPPC molecules. The negative bilayer, which is a mixture of DPPC and DPPG, was obtained by randomly substituting DPPC molecules with DPPG. Together, the neutral and negative bilayer are presented here to model typical mammalian cell membranes that tend to have an overall negative electric feature.

For each bilayer, we created a cubic simulation box in which the bilayer is submerged in water. The dimensions of the box are 24.1 × 24.1 × 17.2 nm^3 with 1152 lipid molecules and approximately 50300 water molecules. First, the water−bilayer systems were equilibrated for 10 ns. After equilibration, the AuNPs were inserted into the water 7 nm above the bilayer center. Counterions were subsequently generated to neutralize the AuNP−bilayer systems. The AuNPs and the bilayers were then harmonically constrained for 10 ns to equilibrate water and ions. After the constraint run, the AuNPs and the bilayers were released to interact freely. Each unbiased production run was performed for 40 ns with a time step of 20 fs. For biased simulation, the umbrella sampling technique[42] and weighted histogram analysis method[43] were applied to calculate the PMF. Because of the smoothed energy barrier of the CG model, the effective sampling time is four times longer than the marked time.[28] All simulation times mentioned in the paper are the effective time.

Temperature was controlled at 305 K and the Berendsen thermostat pressure coupling[44] was applied to maintain the pressure at 1 bar by freely adjusting three dimensions of the box. The cut off radii of both van der Waals and short-ranged Coulombic interactions are 1.2 nm. A particle mesh Ewald summation (PME) method was employed to account for the long-ranged Coulombic interactions.[25,45] Ions have a reduced charge of 0.7 in order to mimic the implicit screening of the first hydrogen shell.[28] All CG MD simulations were performed using the GROMACS 3.3.2 package.[46]

Acknowledgment. The supports of the National Natural Science Foundation (10721062, 50679013, 90715037, 10902021), the 111 Project (No.B08014), the Program for Changjiang Scholars and Innovative Research Team in University (PCSIRT), and the National Key Basic Research Special Foundation of China (2010CB832704) are gratefully acknowledged.

Supporting Information Available: Construction of the CG AuNP model, free energy simulations, calculation of the bilayer properties, and system potential energy fluctuations. This material is available free of charge *via* the Internet at http://pubs.acs.org.

REFERENCES AND NOTES

1. Ghosh, P.; Han, G.; De, M.; Kim, C. K.; Rotello, V. M. Gold Nanoparticles in Delivery Applications. *Adv. Drug Delivery Rev.* **2008**, *60*, 1307–1315.
2. Paciotti, G. F.; Myer, L.; Weinreich, D.; Goia, D.; Pavel, N.; McLaughlin, R. E.; Tamarkin, L. Colloidal Gold: A Novel Nanoparticle Vector for Tumor Directed Drug Delivery. *Drug Delivery* **2004**, *11*, 169–183.
3. Rosi, N. L.; Mirkin, C. A. Nanostructures in Biodiagnostics. *Chem. Rev.* **2005**, *105*, 1547–1562.
4. Peer, D.; Karp, J. M.; Hong, S.; Farokhzad, O. C.; Margalit, R.; Langer, R. Nanocarriers as an Emerging Platform for Cancer Therapy. *Nat. Nanotechnol.* **2007**, *2*, 757–760.
5. El-Sayed, I. H.; Huang, X. H.; El-Sayed, M. A. Selective Laser Photo-thermal Therapy of Epithelial Carcinoma using Anti-EGFR Antibody Conjugated Gold Nanoparticles. *Cancer Lett.* **2006**, *239*, 129–135.
6. Sandhu, K. K.; McIntosh, C. M.; Simard, J. M.; Smith, S. W.; Rotello, V. M. Gold Nanoparticle-Mediated Transfection of Mammalian Cells. *Bioconjugate Chem.* **2002**, *13*, 3–6.
7. Prashant, K. J.; El-sayed, I. H.; El-Sayed, M. A. Au Nanoparticles Target Cancer. *Nanotoday* **2007**, *2*, 18–29.
8. Shukla, R.; Bansal, V.; Chaudhary, M.; Basu, A.; Bhonde, R. R.; Sastry, M. Biocompatibility of Gold Nanoparticles and Their Endocytotic Fate Inside the Cellular Compartment: A Microscopic Overview. *Langmuir* **2005**, *21*, 10644–10654.
9. Allen, T. M.; Cullis, P. R. Drug Delivery Systems: Entering the Mainstream. *Science* **2004**, *303*, 1818–1822.
10. Oberdörster, G.; Oberdörster, E.; Oberdörster, J. Nanotoxicology: An Emerging Discipline Evolving from Studies of Ultrafine Particles. *Environ. Health. Perspect.* **2005**, *113*, 823–39.
11. Nel, A.; Xia, T.; Mädler, L.; Li, N. Toxic Potential of Materials at the Nanolevel. *Science* **2006**, *311*, 622–627.
12. Leroueil, P. R.; Hong, S.; Mecke, A.; Baker, J. R., Jr.; Orr, B. G.; Banaszak Holl, M. M. Nanoparticle Interaction with Biological Membranes: Does Nanotechnology Present a Janus Face. *Acc. Chem. Res.* **2007**, *40*, 335–342.
13. Cho, E. C.; Xie, J.; Wurm, P. A.; Xia, Y. Understanding the Role of Surface Charges in Cellular Adsorption *versus* Internalization by Selectively Removing Gold Nanoparticles on the Cell Surface with a I_2/KI Etchant. *Nano Lett.* **2009**, *9*, 1080–1084.
14. Chithrani, B. D.; Ghazani, A. A.; Chan, W. C. Determining the Size and Shape Dependence of Gold Nanoparticle Uptake into Mammalian Cells. *Nano Lett.* **2006**, *6*, 662–668.
15. Peelta, C.; Labhasetwar, V. Effect of Molecular Structure of Cationic Surfactants on Biophysical Interactions of Surfactant-Modified Nanoparticles with a Model Membrane and Cellular Uptake. *Langmuir* **2009**, *25*, 2369–2377.
16. Hauck, T. S.; Ghazani, A. A.; Chan, W. C. Assessing the Effect of Surface Chemistry on Gold Nanorod Uptake, Toxicity, and Gene Expression in Mammalian Cells. *Small* **2008**, *4*, 153–159.
17. Verma, A.; Uzun, O.; Hu, Y.; Hu, Y.; Han, H. S.; Watson, N.; Chen, S.; Irvine, D. J.; Stellacci, F. Surface-Structure-Regulated Cell-Membrane Penetration by Monolayer-Protected Nanoparticles. *Nat. Mater.* **2008**, *7*, 588–595.
18. Connor, E. E.; Mwamuka, J.; Gole, A.; Murphy, C. J.; Wyatt, M. D. Gold Nanoparticles Are Taken up by Human Cells but Do Not Cause Acute Cytotoxicity. *Small* **2005**, *3*, 325–327.
19. Aillon, K. L.; Xie, Y.; El-Gendy, N.; Berkland, C. J.; Forrest, M. L. Effects of Nanomaterial Physicochemical Properties on *in Vivo* Toxicity. *Adv. Drug Delivery Rev.* **2009**, *61*, 457–466.
20. Lewinski, N.; Colvin, V.; Drezek, R. Cytotoxicity of Nanoparticles. *Small* **2008**, *4*, 26–49.
21. Verma, A.; Stellacci, F. Effect of Surface Properties on Nanoparticle−Cell Interactions. *Small* **2010**, *6*, 12–21.
22. Luedtke, W. D.; Landman, U. Structure and Thermodynamics of Self-Assembled Monolayers on Gold Nanocrystallites. *J. Phys, Chem. B* **1998**, *102*, 6566–6572.
23. Schapotschnikow, P.; Pool, R.; Vlugt, T. J. H. *Nano Lett.* **2008**, *8*, 2930–2934.
24. Wallace, E. J.; Sansom, M. S. Molecular Simulations of Interacting Nanocrystals. *Nano Lett.* **2008**, *8*, 2751–2756.
25. Lee, H.; Larson, R. G. Molecular Dynamics Simulations of PAMAM Dendrimer-Induced Pore Formation in DPPC Bilayers with a Coarse-Grained Model. *J. Phys. Chem. B* **2006**, *110*, 18204–18211.
26. Wong-Ekkabut, J.; Baoukina, S.; Triampo, W.; Tang, I. M.; Tieleman, D. P.; Monticelli, L. Computer Simulation Study of Fullerene Translocation Through Lipid Membranes. *Nat. Nanotechnol.* **2008**, *3*, 363–368.
27. Voet, D.; Voet, J. G. *Biochemistry;* John Wiley and Sons, Inc.: New York, 1995.
28. Marrink, S. J.; de Vries, A. H.; Mark, A. E. Coarse Grained Model for Semiquantitative Lipid Simulations. *J. Phys. Chem. B* **2004**, *108*, 750–760.
29. Leontiadou, H.; Mark, A. E.; Marrink, S. J. Molecular Dynamics Simulation of Hydrophilic Pores in Lipid Bilayers. *Biophys. J.* **2004**, *86*, 2156–2164.
30. Kim, C. K.; Ghosh, P.; Pagliuca, C.; Zhu, Z. J.; Menichetti, S.; Rotello, V. M. Entrapment of Hydrophobic Drugs in Nanoparticle Monolayers with Efficient Release into Cancer Cells. *J. Am. Chem. Soc.* **2009**, *131*, 11360–11361.
31. Ginzburg, V. V.; Balijepalli, S. Modeling the Thermodynamics of the Interaction of Nanoparticles with Cell Membranes. *Nano Lett.* **2007**, *7*, 3716–3722.
32. Wang, B.; Zhang, L.; Bae, S. C.; Granick, S. Nanoparticle-Induced Surface Reconstruction of Phospholipid Membranes. *Proc. Natl. Acad. Sci. U.S.A.* **2008**, *105*, 18171–18175.
33. Leroueil, P. R.; Berry, S. A.; Duthie, K.; Han, G.; Rotello, V. M.; McNerny, D. Q.; Baker, J. R., Jr.; Orr, B. G.; Banaszak Holl, M. M. Wide Varieties of Cationic Nanoparticles Induce Defects in Supported Lipid Bilayers. *Nano Lett.* **2008**, *8*, 420–424.
34. Hong, S.; Leroueil, P. R.; Janus, E. K.; Peters, J. L.; Kober, M. M.; Islam, M. T.; Orr, B. G.; Baker, J. R., Jr.; Banaszak Holl, M. M. Interaction of Polycationic Polymers with Supported Lipid Bilayers and Cells: Nanoscale Hole Formation and Enhanced Membrane Permeability. *Bioconjugate Chem.* **2006**, *17*, 728–734.
35. Mukherjee, S.; Ghosh, R. N.; Maxfield, F. R. Endocytosis. *Physiol. Rev.* **1997**, *77*, 759–803.
36. Nel, A. E.; Mädler, L.; Velegol, D.; Xia, T.; Hoek, E. M.; Somasundaran, P.; Klaessig, F.; Castranova, V.; Thompson, M. Understanding Biophysicochemical Interactions at the Nano−Bio Interface. *Nat. Mater.* **2009**, *8*, 543–557.
37. McIntosh, T. J.; Simon, S. A. Roles of Bilayer Material Properties in Function and Distribution of Membrane

Proteins. *Annu. Rev. Biophys. Biomol. Struct.* **2006**, *35*, 177–198.
38. Monticelli, L.; Kandasamy, S. K.; Periole, X.; Larson, R. G.; Tieleman, D. P.; Marrink, S. J. The MARTINI Coarse-Grained Force Field: Extension to Proteins. *J. Chem. Theory and Comput.* **2008**, *4*, 819–834.
39. Whetten, R. L.; Khoury, J. T.; Alvarez, M. M.; Murthy, S.; Vezmar, I.; Wang, Z. L.; Stephens, P. W.; Cleveland, C. L.; Luedtke, W. D.; Landman, U. Nanocrystal Gold Molecules. *Adv. Mater.* **1996**, *8*, 428–433.
40. Adams, J. B.; Foiles, S. M.; Wolfer, W. G. Self-Diffusion and Impurity Diffusion of fcc Metals Using the Five-Frequency Model and the Embedded Atom Method. *J. Mater. Res.* **1988**, *4*, 102–112.
41. Terrill, R. H.; Postlethwaite, T. A.; Chen, C. H.; Poon, C. D.; Terizis, A.; Chen, A.; Hutchison, J. E.; Clark, M. R.; Wignall, G.; Londono, J. D.; *et al*. Monolayer in Three Dimensions: NMR, SAXS, Thermal, and Electron Hopping Studies of Alkanethiol Stabilized Gold Clusters. *J. Am. Chem. Soc.* **1995**, *117*, 12537–12548.
42. Torrie, G. M.; Valleau, J. P. Nonphysical Sampling Distribution in Monte Carlo Free Energy Estimation: Umbrella Sampling. *J. Comput. Phys.* **1977**, *23*, 187–199.
43. Kumar, S.; Bouzida, D.; Swendsen, R. H.; Kollman, P. A.; Rosenberg, J. M. The Wighted Histogram Analysis Method for Free-Energy Calculations on Biomolecules. 1. The Method. *J. Comput. Chem.* **1992**, *13*, 1011–1021.
44. Berendsen, H. J. C.; Postma, J. P. M.; Van Gunsteren, W. F.; Dinola, A.; Haak, J. R. Molecular Dynamics with Coupling to an External Bath. *J. Chem. Phys.* **1984**, *81*, 3684–3690.
45. Essmann, U. L.; Perera, L.; Berkowitz, M. L.; Darden, T.; Lee, H.; Pedersen, L. G. A Smooth Particle Mesh Ewald Method. *J. Chem. Phys.* **1995**, *103*, 8577–8592.
46. Van Der Spoel, D.; Lindahl, E.; Hess, B.; Groenhof, G.; Mark, A. E.; Berendsen, H. J. C. GROMACS: Fast, Flexible and Free. *J. Comput. Chem.* **2005**, *26*, 1701–1718.